



Prediction model of peripheral milling surface geometry considering cutting force and vibration

Boling Yan¹ · Lida Zhu¹ · Changfu Liu¹

Received: 28 April 2020 / Accepted: 9 August 2020 / Published online: 24 August 2020
© Springer-Verlag London Ltd., part of Springer Nature 2020

Abstract

Milling surface quality is an important factor to assess the performance of a product, which is usually affected by cutting parameters. This paper presents a novel model of peripheral milling surface topography considering tool vibration. The model used the idea of discretization by introducing the milling dynamics and ignored the effect of tool wear, tilting, and thermal deformation. The simulation results were verified and showed good consistence with experimental results. Afterwards, parametric analysis was conducted to investigate the impact of process parameters and showed that feed per tooth impacts most on the surface roughness while axial depth of cut has the least impact. The presented method enables researchers to predict the peripheral milling surface before processing. Moreover, the method helps to build the formula of surface roughness to conduct the parameter optimization.

Keywords Milling dynamics · Surface topography · Tool vibration · Process parameters · Modal analysis

1 Introduction

In the field of advanced manufacturing, machined surface quality is an important indicator of product performance. Milling surface quality suggests the machining accuracy and has impact on the abrasive resistance, surface finish, thermal conductivity, and parts' service life [1]. The milling surface topography indicates the milling surface quality and is closely related to milling force. Usually, the increasing of cutting parameters leads to the growth of the milling force, which will in turn cause the tool to deform and vibrate, and the milling geometry varies due to the change of process parameters. However, the process parameters must be controlled within a proper range to avoid chatter. According to the regenerative chatter theory, if the cutting force exceeds and extends where the stiffness of milling system is too weak to maintain the stable vibration, chatter will happen. Chatter can destroy the

machined surface and leave chatter marks [2]. This article aims to build the prediction model of peripheral milling surface under chatter-free machining condition, and the model does not include chatter condition.

In recent years, many researchers have established the surface geometry model of milling process [3–9]. Omar et.al [4] introduced a model to predict surface topography as well as cutting force including effect of tool runout, tool deflection, system dynamics, and tool tilting. Yang and Liu [5] proposed a prediction model of peripheral milling surface topography considering plastic deformation. After experiment and sensitivity analysis, it is found that the effect of cutting speed can be neglected to the surface topography and deflection of tool affects most on the surface profile. Arizmendi et.al [7, 8] presented the model of both peripheral and face milling surface topography and the simulated results showed good agreements with experiments. Milling surface roughness is also a research hotspot, and many studies focused on this topic [10–15]. Zhang et.al [10] predicted the surface roughness through the Gaussian process regression (GPR) considering spindle speed, feed rate, and depth of cut. Frequency spectrum was conducted based on 3D map of surface roughness, and it was found that tool vibration is a critical factor affecting the surface quality. Bolar

✉ Lida Zhu
neulidazhu@163.com

¹ School of Mechanical Engineering and Automation, Northeastern University, Shenyang 110819, People's Republic of China

et.al [11] systematically measured milling force and surface roughness of thin-walled workpiece, which were used to conduct variance and regression analysis and to predict the cutting force and surface roughness. The influence of cutting parameters as well as tool diameter was analyzed through response surface methodology.

Above all, cutting force and tool vibration have great impact on the surface topography and the process parameters should be discussed to obtain their impact on the milling surface. Vibration affects and determines the machined surface, which should be limited within an ideal range. In their works, Wan et.al [16, 17] used dynamic vibration absorber to suppress vibration in milling of plate-like and cylindrical workpiece. Cutting force coefficients enable researchers to take the relative hardness of workpieces and tools into account through prediction model, and the cutting force and vibration will be determined once the machine tool, mill, workpiece, and the cutting parameters are settled. The cutter and workpiece were discrete along axial direction to get the contour of section. Then, the displacement of the tool was added to the contour according to milling dynamics. After the verification of simulation, the process parameters were investigated to study their effects on the machined surface. The presented method could more accurately predict the machined surface, and the complexity of the corresponding algorithm is relatively low. Therefore, the algorithm can achieve both accuracy and efficiency. In addition, the model presented a method to calculate the surface roughness, which was proved to be

effective to conduct parameter optimization before processing begins.

The reminder of this article is organized as follows. In Section 2, the surface generation model considering tool vibration is presented. Then, the modal test and modal analysis are conducted to acquire the processing ability of the machine tool in Section 3. In Section 4, the surface simulation results basing on the recognized modal parameters are proved to be accurate through milling experiment. Conclusions are discussed and listed in Section 5.

2 Surface generation model of peripheral milling

2.1 Surface generation model

In ideal peripheral milling process, machined surface can be seen as a reflection of relative movement between tool and workpiece, and the milling chips are removed due to the hardness difference to the cutter. If the milling force continues to enlarge, the deformation and vibration should be taken into account. The formation of reproduced surface is shown in Fig. 1.

As in Fig. 1, the reproduced surface contains two face—end face and side face—and the side face meets the motion of rotating and feed movement, which arouse the most concerning in peripheral milling. According to previous researchers [18, 19], the mixture of feed motion and revolution

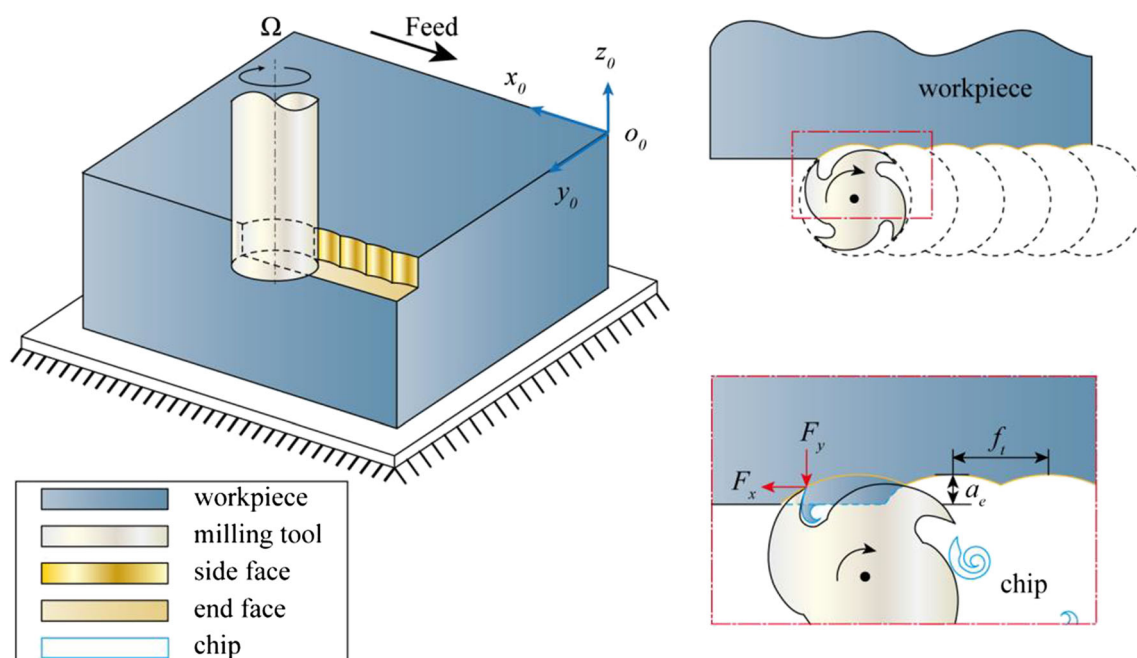


Fig. 1 The formation of peripheral milling surface

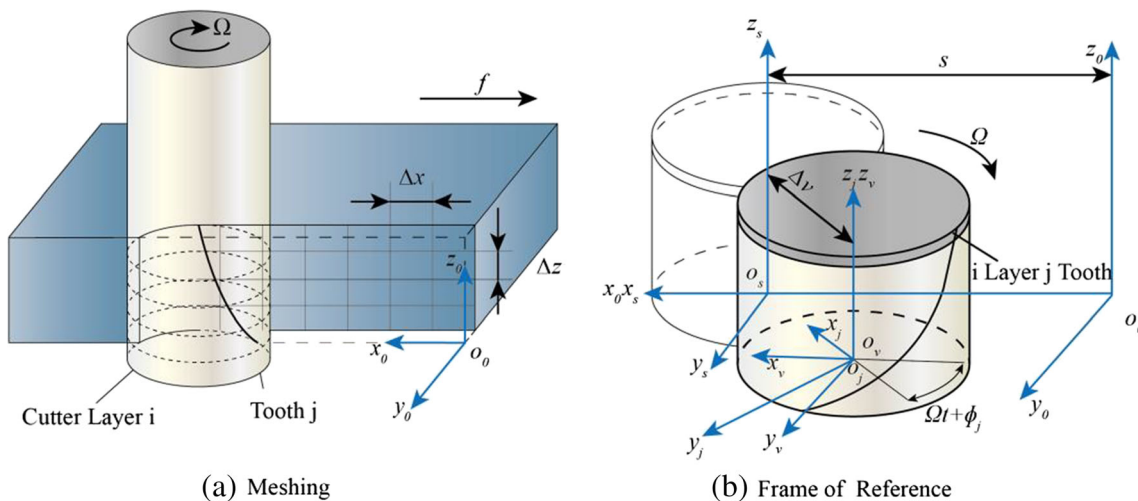


Fig. 2 The Cartesian coordinate system of the cutting edge trajectory equation

creates the secondary cycloidal path of tool teeth. Due to the spiral form of cutting edge, this kind of movement varies along the different axial depth.

Therefore, if tool and workpiece are discretized in the axial direction as well as feed direction and the relative trajectory of tool and workpiece is obtained, the surface

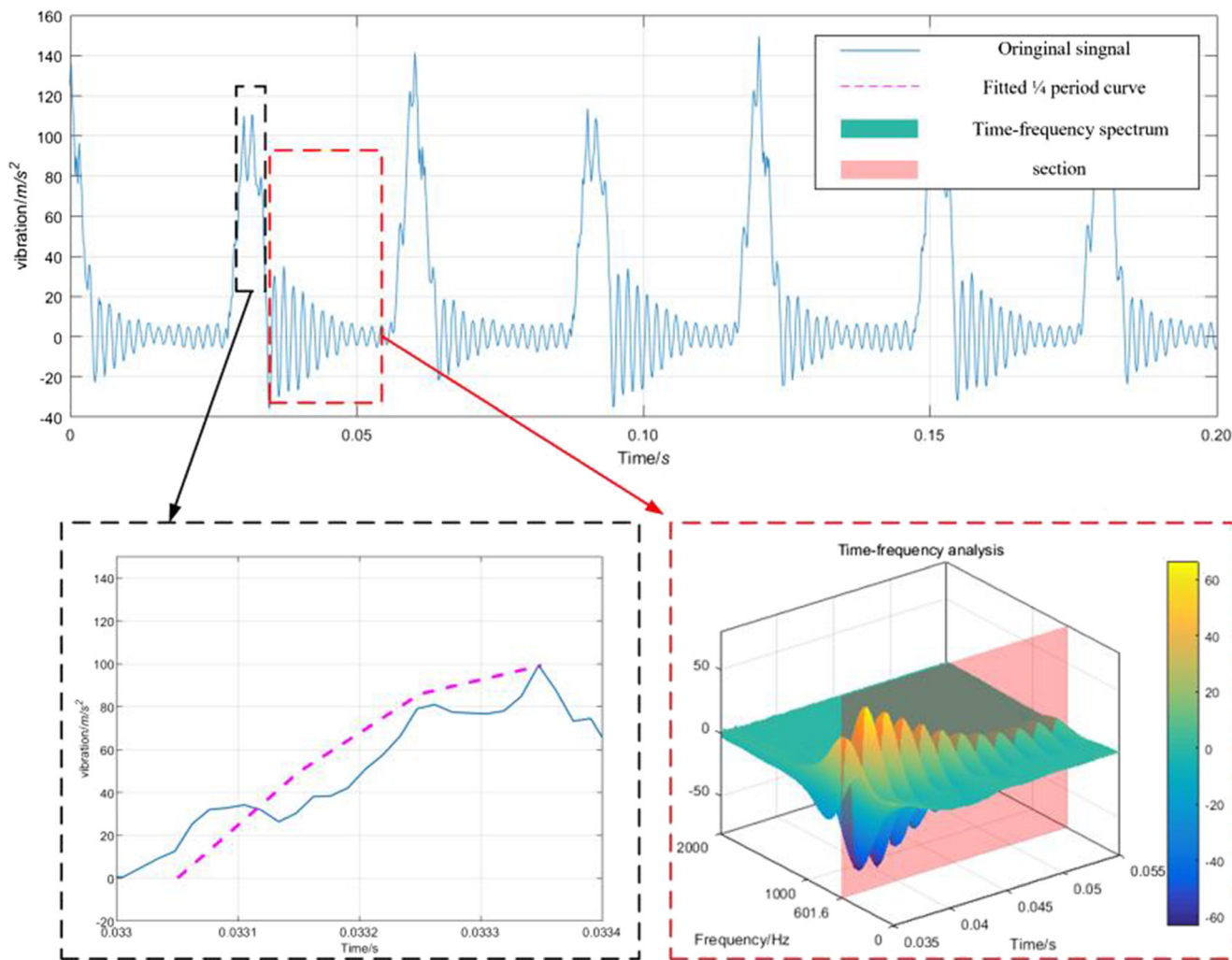


Fig. 3 Description of vibration signal by STFT analysis, $a_p = 4$ mm, $a_e = 0.5$ mm, $f = 100$ mm/min, $n = 1000$ rpm, $D = 12$ mm, $N_t = 2$

topography of the machined workpiece can be acquired under certain parameters. The discretization of tool and workpiece and the tool coordinate system are established in Fig. 2.

In Fig. 2, four sets of Cartesian coordinate systems are set as follows.

1. $O_0X_0Y_0Z_0$, workpiece coordinate T_0
2. $O_sX_sY_sZ_s$, spindle coordinate T_s , and transformation to T_0 is $T_0 = T_{0,s}(s)T_s$
3. $O_vX_vY_vZ_v$, vibration coordinate T_v . Corresponding transformation is $T_{s,v}(\Delta v)$
4. $O_jX_jY_jZ_j$, rotation coordinate T_j . Transformation term is $T_{v,j}(\Omega)$

If the rotation coordinate T_j and all the transformation above are correctly represented, the relative motion trajectory of the tool and the workpiece can be deduced accordingly. The coordinate T_j is the geometry of tool j th tooth, which can be expressed as spiral in polar form, as in Eq. (1).

$$\begin{bmatrix} x_j \\ y_j \\ z_j \\ 1 \end{bmatrix} = \begin{bmatrix} R\cos\theta \\ R\sin\theta \\ R\theta/\tan\beta \\ 1 \end{bmatrix} \tag{1}$$

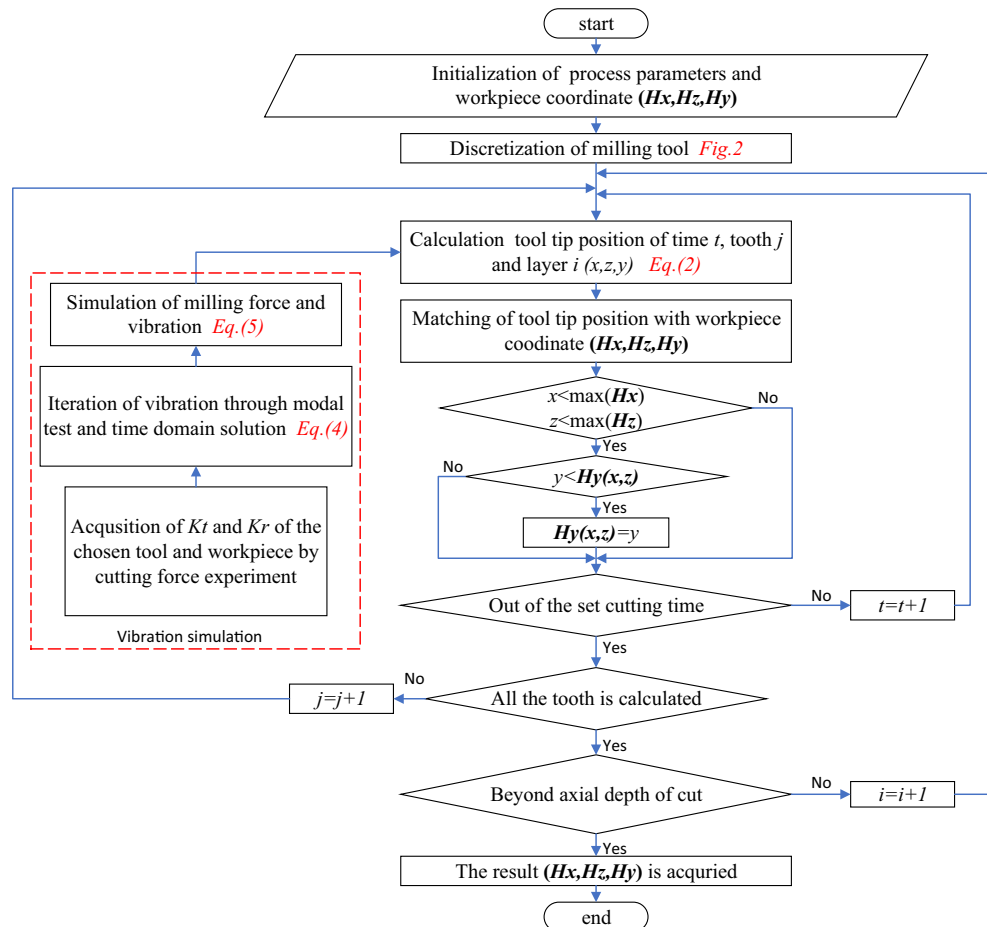
where R is the radius of tool, θ is the coordinate parameter, and β is the helix angle of the milling cutter. Thus, the trajectory of the tool and the workpiece is obtained as in Eq. (2)

$$T_0 = T_{0,s}(s) \times T_{s,v}(\Delta v) \times T_{v,j}(\Omega) \times T_j \tag{2}$$

where $T_{0,s}(s)$ and $T_{s,v}(\Delta v)$ represent the relative trace and the amount of tool vibration respectively. The equations of $T_{0,s}(s)$ and $T_{s,v}(\Delta v)$ are given as follows.

$$\begin{aligned} T_{0,s}(s) &= \begin{bmatrix} 1 & 0 & 0 & x(t) \\ 0 & 1 & 0 & y(t) \\ 0 & 0 & 1 & z(t) \\ 0 & 0 & 0 & 1 \end{bmatrix}, T_{s,v}(\Delta v) \\ &= \begin{bmatrix} 1 & 0 & 0 & \Delta x(t) \\ 0 & 1 & 0 & \Delta y(t) \\ 0 & 0 & 1 & 0 \\ 0 & 0 & 0 & 1 \end{bmatrix} \end{aligned} \tag{3}$$

Fig. 4 Flow chart of the surface topography simulation in the peripheral milling process



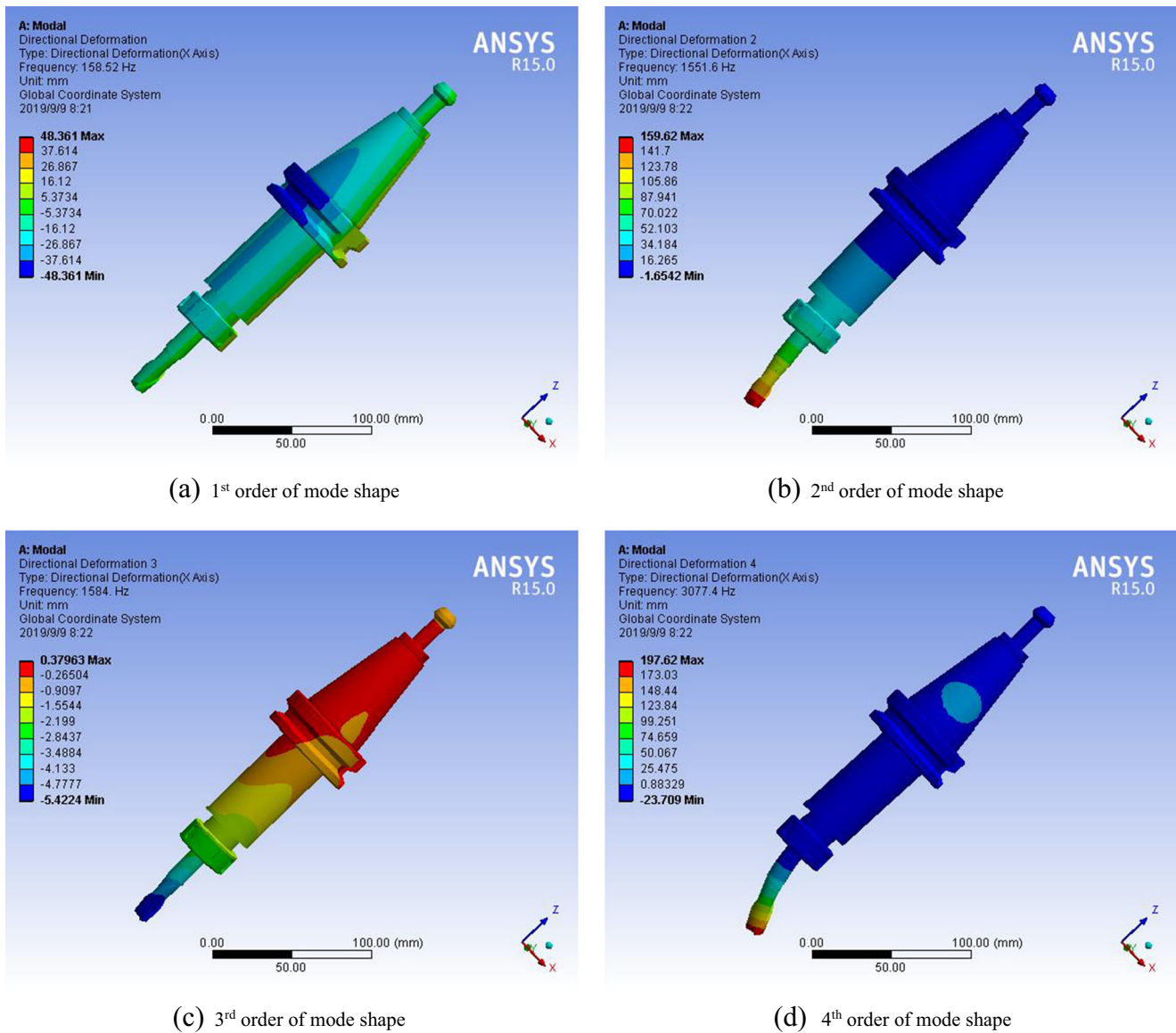


Fig. 5 Modal simulation via finite element analysis (ANSYS 17.2)

In Eq. (3), $x(t)y(t)z(t)$ is the feed movement in X , Y , and Z directions, $\Delta x(t)\Delta y(t)$ is tool vibration in the corresponding direction, Ω is the spindle speed, and ϕ_j is the respective angle of tooth. The equation of $T_{0,s}(s)$ and workpiece coordinate T_0 in peripheral milling can be expressed as follows.

Table 1 Tool parameters and milling force coefficients

Name	Value
Number of tooth N_t	2
Tool diameter D	12 mm
Tool length L	75 mm
Cutting edge length L_c	30 mm
K_t	1189 MPa
K_r	158.8 MPa

$$T_{0,s}(s) = \begin{bmatrix} 1 & 0 & 0 & f_i(t) \\ 0 & 1 & 0 & R \\ 0 & 0 & 1 & 0 \\ 0 & 0 & 0 & 1 \end{bmatrix}$$

i. Down milling

$$T_{v,j}(\Omega) = \begin{bmatrix} \cos(\Omega t + \phi_j) & \sin(\Omega t + \phi_j) & 0 & 0 \\ -\sin(\Omega t + \phi_j) & \cos(\Omega t + \phi_j) & 0 & 0 \\ 0 & 0 & 1 & 0 \\ 0 & 0 & 0 & 1 \end{bmatrix}, T_0 = \begin{bmatrix} f(t) + R\cos(\Omega t + \phi_j - \theta) + \Delta x \\ R - R\sin(\Omega t + \phi_j - \theta) + \Delta y \\ R\theta / \tan\beta \\ 1 \end{bmatrix} \tag{4}$$

Table 2 Results of modal parameter identification

Modal orders	Natural frequency (Hz)	Damping ratio (%)	Stiffness (N/m)
Cutter <i>x</i> direction 1st	1013	3.08	1.10e7
Cutter <i>x</i> direction 2nd	1550	3.23	1.74e7
Cutter <i>x</i> direction 3rd	2825	3.54	1.15e7
Cutter <i>y</i> direction 1st	1013	1.83	7.30e6
Cutter <i>y</i> direction 2nd	1700	2.79	9.21e6
Cutter <i>y</i> direction 3rd	2888	1.73	1.67e7

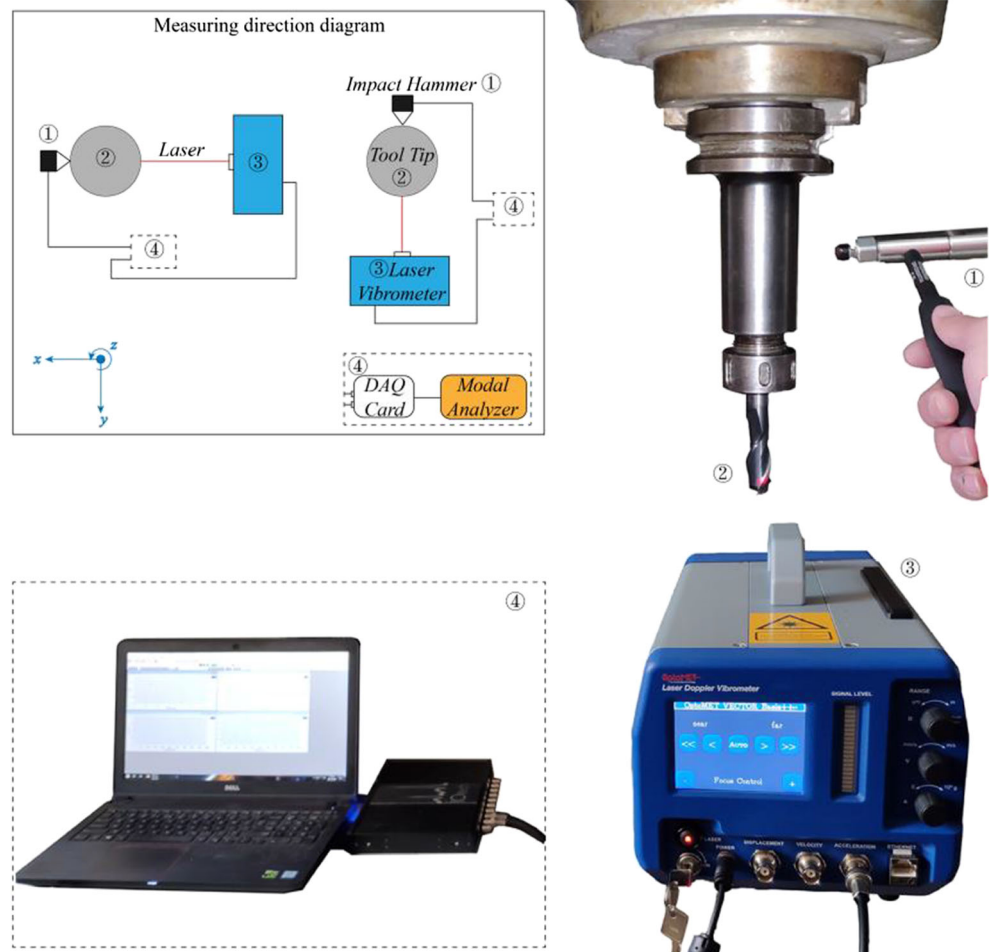
ii. Up milling

$$T_{v,j}(\Omega) = \begin{bmatrix} \cos(\Omega t + \phi_j) & -\sin(\Omega t + \phi_j) & 0 & 0 \\ \sin(\Omega t + \phi_j) & \cos(\Omega t + \phi_j) & 0 & 0 \\ 0 & 0 & 1 & 0 \\ 0 & 0 & 0 & 1 \end{bmatrix}, T_0 = \begin{bmatrix} ft(t) + R\cos(\Omega t + \phi_j - \theta) + \Delta x \\ R + R\sin(\Omega t + \phi_j - \theta) + \Delta y \\ R\theta/\tan\beta \\ 1 \end{bmatrix}$$

2.2 Description of tool vibration

As discussed in Eq. (2), the transformation term $T_{s,v}(\Delta v)$ should be systematically discussed. Under ideal conditions, milling tool is simplified as a cantilever beam. The vibration trace of tool can then be considered as trace of tool center position (TCP). Forced vibration occurs under stable cutting machine tool [18], which is closely related to the dynamics of machine tool [20, 21]. Figure 3 shows the vibration of a thin-walled workpiece. The vibration is measured by an accelerometer attached to the workpiece.

Fig. 6 The formation of peripheral milling surface



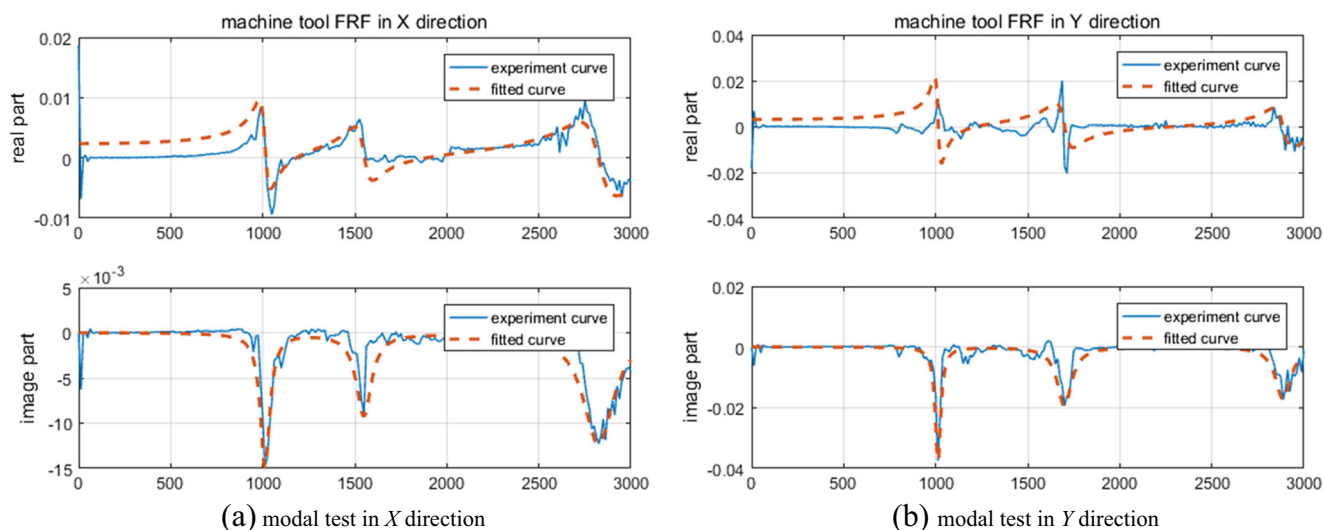


Fig. 7 Comparison of experimental transfer function curve and fitted curve

As in Fig. 3, tool wear can be easily recognized accordingly. If the tool wear is ignored, the tool vibrates periodically, and the changing frequency is identical to the tooth passing frequency ($\omega_T = 2\pi\Omega N_t/60$) [18]. The vibration in one period can be decomposed into two stages, one is caused by cutting and the other is a kind of attenuated vibration. The first part can be described as sine wave, whose time ratio to the whole cycle equals to $\tau = 2 \arccos[(R - a_e)/R]/\pi$. Combined STFT analysis with vibration knowledge, the frequency of the damping decay is closely related to the first order natural frequency of the processing system ω_n

Under ideal cutting condition without considering tool wear and structural mode coupling effect, the vibration Δx or Δy can be expressed as Eq. (5).

$$\Delta x(\Delta y) = \begin{cases} \Delta A \sin(\pi t / 2t_k), & \frac{60k}{\Omega N_t} \leq t < t_k \\ \Delta A \sin(2\pi\omega_n(t-t_k)) / [2\pi\omega_n(t-t_k)], & t_k \leq t < \frac{60(k+1)}{\Omega N_t} \end{cases} \quad k = 0, 1, 2 \dots \quad (5)$$

where ΔA is the amplitude of displacement and has a relationship with cutting force coefficients. $t_k = \frac{60(k+\tau)}{\Omega N_t}$, where $\tau = 2 \arccos[(R - a_e)/R]/\pi$. The forced vibration equation of a two-DOF where x and y are perpendicular to each other is expressed as Eq. (6).

$$M \begin{bmatrix} m_x & 0 \\ 0 & m_y \end{bmatrix} K \begin{bmatrix} k_x & 0 \\ 0 & k_y \end{bmatrix} C \begin{bmatrix} c_x & 0 \\ 0 & c_y \end{bmatrix} \{s\} = \begin{bmatrix} x(t) \\ y(t) \end{bmatrix} \quad \{F\} = \begin{bmatrix} F_x(t) \\ F_y(t) \end{bmatrix} \quad (6)$$

where $F_x(t)$ and $F_y(t)$ are the combination of two stages in Eq. (4). According to superposition principle of linear system, the solution of Eq. (6) is the superposition of vibration in stage one and in stage two. The first term of cutting force is harmonic, leading to a forced vibration. The second term can be

transformed into Fourier series, and the solution is the sum of vibration aroused by these series. The numerical solution of second order differential equation can be deduced through MATLAB.

2.3 Flow of surface generation simulation under plane machining

The milling surface generation model can be deduced after the tool vibration is obtained. Figure 4 demonstrates the simulation strategy of plane milling surface prediction model: processing parameters as well as the vibration in time domain are input firstly to get the trace of tool tip as Eq. (2). Secondly, the residual height y in time t and layer i is compared with the initial value $H_y(x, z)$. The $H_y(x, z)$ value changes to y if $y \leq H_y(x, z)$. After three-order iterations from t (time) to i (layer), the matrix H_y contains the information of machined surface.

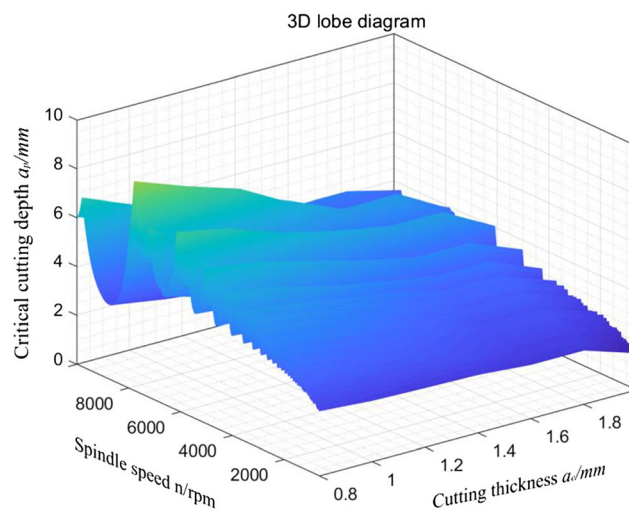


Fig. 8 Three-dimensional lobe diagram

The simulation of vibration is also demonstrated in Fig. 4, where the cutting force coefficients K_t and K_r should be obtained firstly by cutting force experiment. Combining the cutting force coefficients, modal parameters, and Eq. (5), the description of tool vibration is deduced.

3 Modal analysis of machine tool

As presented in Section 2.3, the modal parameters should be obtained to conduct vibration simulation. Therefore, modal test should be conducted to get the surface topography. Solid carbide tool UP210-S2-12030 and aluminum 6061T6 workpiece ($100 \times 50 \times 20 \text{ mm}^3$) are selected to conduct simulation and experiment. Since the workpiece is not a kind of

thin-walled workpiece, its vibration is much smaller than the tool, which is ignored.

Apart from modal parameter recognition, modal finite analysis is also important to get knowledge of mode shape as well as modal test setup.

3.1 Mode shape simulation via finite element

As mentioned above, vibration affects the formation of surface. However, different vibration frequency may have different influence on the surface generation according to their vibration shape. With the help of finite element analysis, the mode shape can be acquired. The results of modal analysis of machine tool holder are demonstrated in Fig. 5.

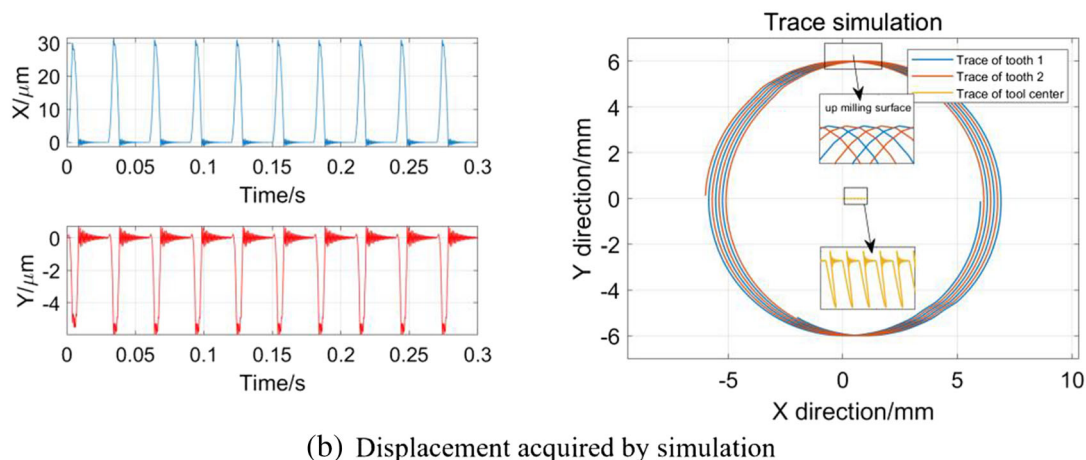
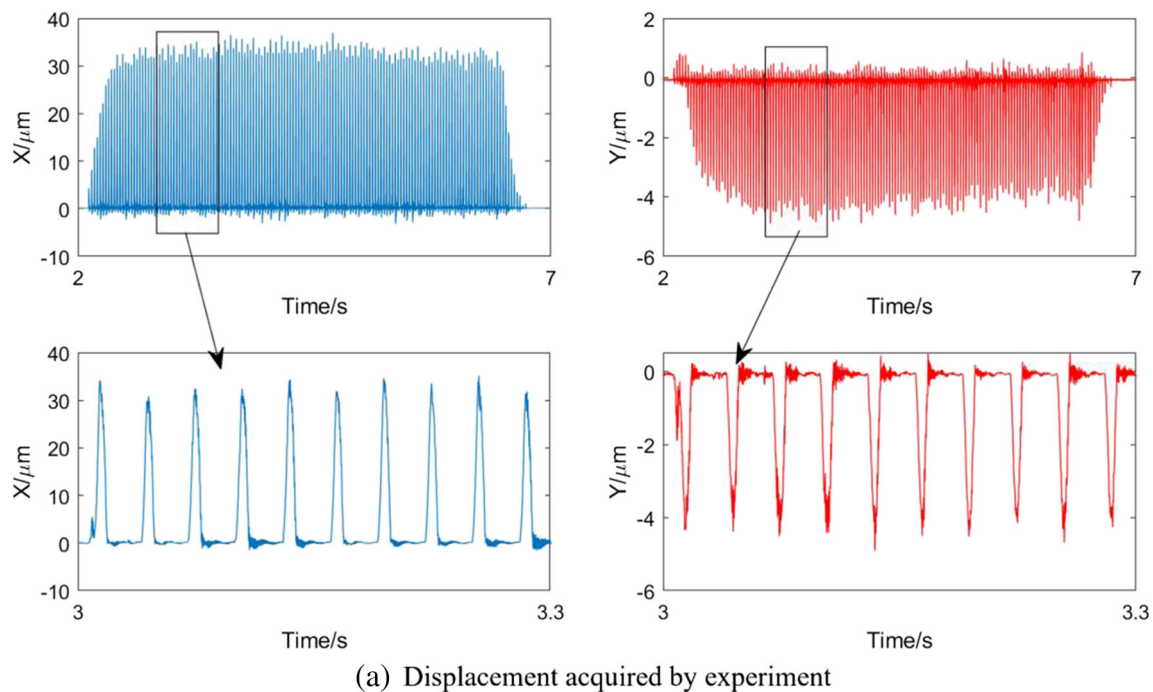


Fig. 9 Simulation of vibration and trace

The spindle is not included in the analysis, so the natural frequency of each mode does not equal to the actual value. As shown in Fig. 5, the directional deformation has maximum amplitude at tool tip in all the modal orders. Therefore, the accelerometer should be placed at tool tip during modal test to get a more convincing result. In addition, the vibration has different shapes according to different spindle speed as well as milling force. When the rotation frequency is close to the natural frequency, the resonance may happen.

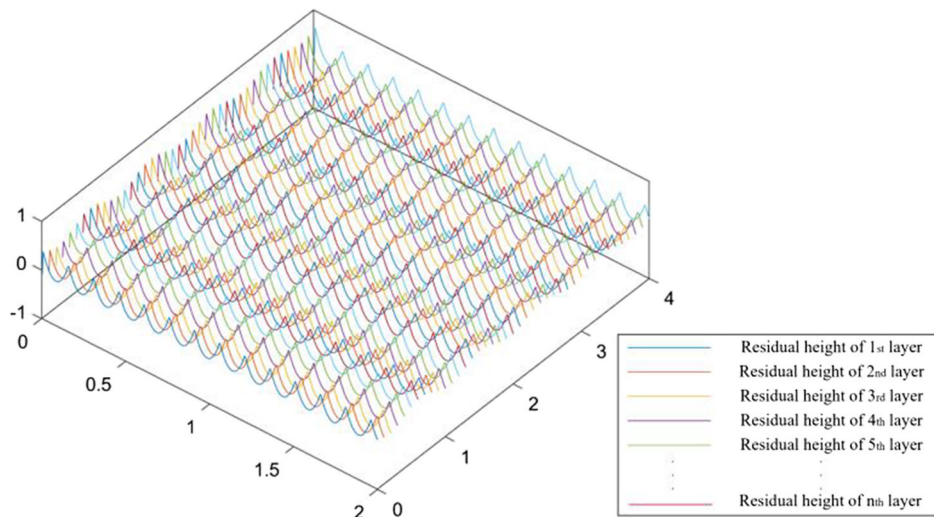
3.2 Modal test and modal parameter identification

The cutting force coefficients have already been acquired through previous work. Table 1 illustrates the tool parameters as well as the force coefficients.

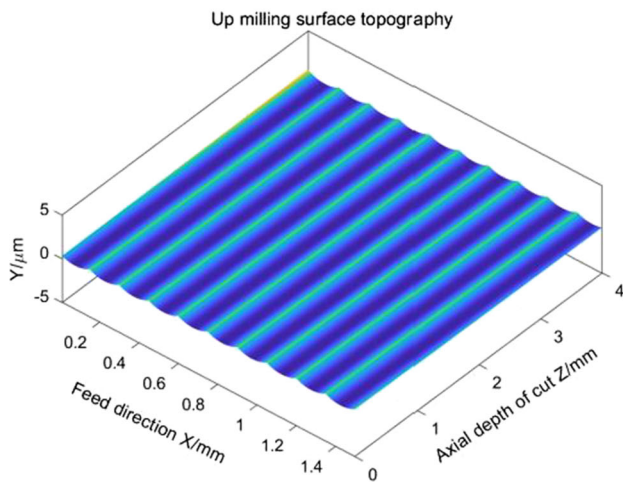
The facilities used to conduct the modal test consist of impact hammer, laser vibrometer, and the data acquisition card.

Figure 6 illustrates the measurement direction of modal test and the experimental devices. As shown in the figure, tool tip is motivated for the relatively low stiffness. Both the hammer force and the acceleration of mill in *X* and *Y* directions is submitted into the modal analyzer to obtain these two direction frequency response functions. The recognized modal parameters are shown in Table 2 and the transfer function curve is shown in Fig. 7.

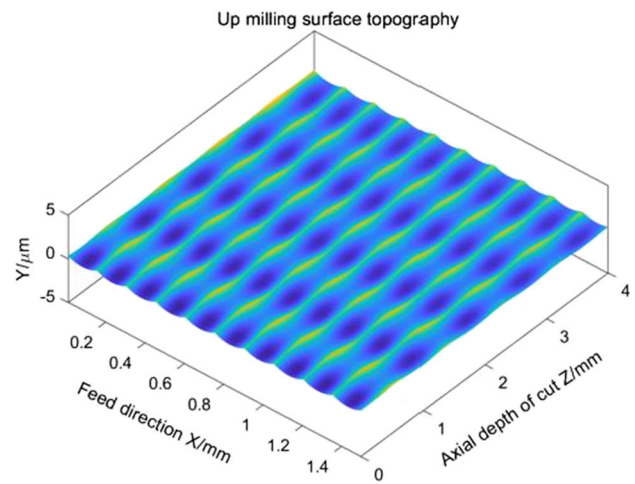
As in Fig. 7, higher order of frequency beyond 3000 Hz is omitted because of its small impact on the dynamics of milling cutter. Comprehensively consider the real part and image part of the fitted curve, the recognition of modal parameters is roughly consistent with the experiment results



(a) Tool tip trace in different tool axial layer



(b) Simulation of surface topography without considering vibration



(c) Simulation of surface topography

Fig. 10 Simulation of surface generation model

4 Results and discussion

4.1 Simulation of tool dynamics and surface topography

Lobe diagram can be depicted according to cutting force coefficients and modal parameters as in Table 1 and Table 2, which is shown in Fig. 8. The cutting thickness is selected within the range from 0.8 to 1.8 mm, and the spindle speed is between 1000 and 10,000 rpm [22].

To conduct experiment and time domain simulation, cutting parameters are chosen as follows. Axial depth of cut a_p is 4 mm, radial depth of cut a_e is 0.5 mm, X direction feed per tooth f_t is 0.3 mm/z, and the spindle speed is 1000 rpm. Up milling is selected to conduct simulation and experiment.

As in Fig. 9(a), vibration has the identical tendency as expressed in Section 2.2 and similar to the result of time domain simulation. Therefore, time domain simulation can be used as illustrated in Fig. 4.

According to spindle speed and the number of teeth, the changing frequency of vibration is $\omega_T = 418.67\text{Hz}$, attenuation frequency equals to $\omega_n = 1013\text{Hz}$. Figure 8(b) demonstrates the formation of i th layer cutter (axial depth $i \times dz$) residual height as well as the displacement of tool center. The residual height forms due to the contour line of the discrete cutter, and synthesizing of these layers leads to the topography of the peripheral milling surface. The simulation result is displayed in Fig. 10 (a), (b), and (c).

As described in Fig. 10, if vibration of the tool is not included, the surface along axial direction is linear, which is the same as Fig. 10(b). When vibration is considered, the surface is wavy along axial direction. The surface roughness is mainly composed of two directions: one is resulted from the motion of feed as well as rotation, which is parallel to the feed

direction. The other is formed because of vibration, which is parallel to the tool axis. If the influence of vibration is ignored, the surface geometry can only be affected by feed per tooth f_t , which is quite inconsistent with the experimental results.

To test the effect of cutting force, a set of simulation was conducted under different chip thickness and feed per tooth, which can be seen in Fig. 11.

Compared with simulation result in Fig. 10, the result of Fig. 11(a) has more feed marks because of the reduction of feed rate. However, it is obvious that the residual height in feed direction and the vibration marks in axial direction are smaller than that of Fig. 10. As in Fig. 11(b), the amount of feed marks keeps the same with Fig. 10, while the vibration marks are much larger than Fig. 10. As we know, milling force increases with the increase of chip thickness or feed per tooth. The conclusion can be drawn from the simulation that with the increase of cutting force and tool vibration amplitude, the surface roughness tends to increase.

4.2 Experimental verification of presented model

To validate the simulation results, a set of cutting test was conducted. The experiment environments are shown in Fig. 12 and the cutting parameters are listed in Table 3

The milling surface is measured through laser scanning confocal microscope LEXTOLS 4100. The comparison of simulation and experiment under same cutting parameters is shown in Fig. 13.

Note that the unit in experimental results is μm . As demonstrated in Fig. 13, the topography of peripheral milling and simulation has something in common. Firstly, the marks left on the feed direction have the same amount under same scale when feed per tooth is identical. Secondly, the surface along

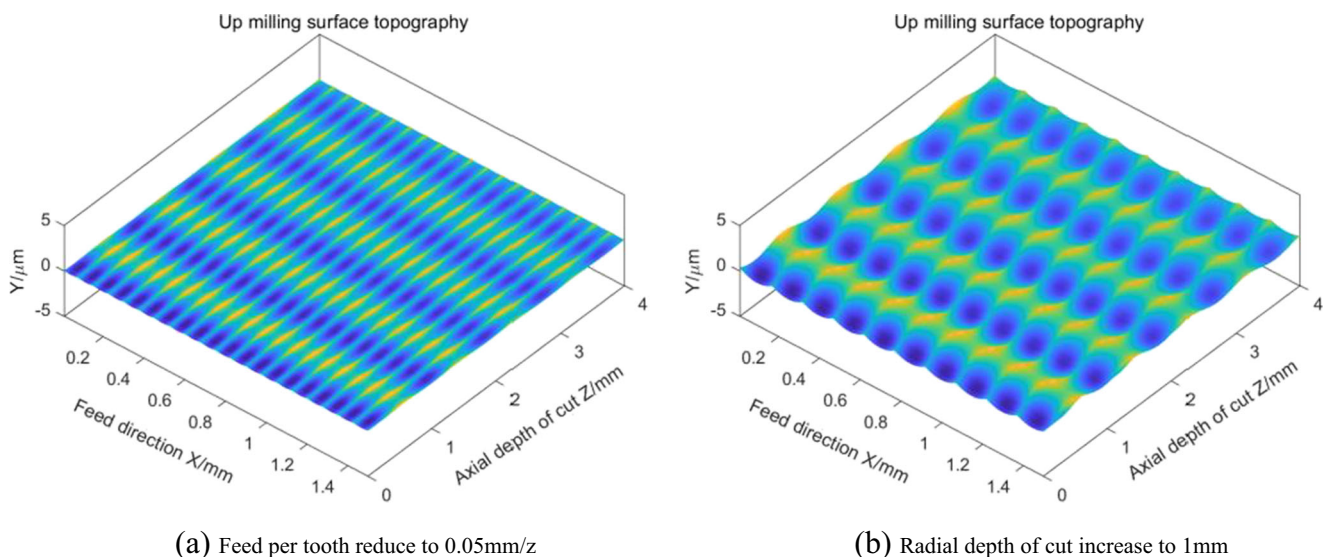
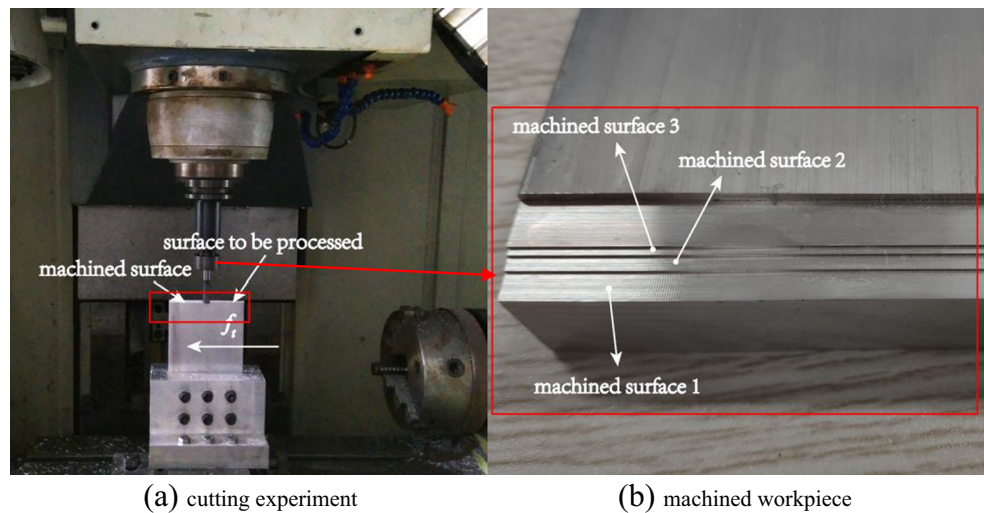


Fig. 11 Simulation of surface generation model

Fig. 12 Cutting experiment and workpiece



tool axis changes periodically. Thus, we can say that the model presented is effective to simulate the surface topography.

There are subtle differences between simulation and experiment, however, which may be because of tool tilt, scratch, or burning of workpiece and other reasons. Therefore, surface roughness was chosen as an indicator to examine the accuracy of the model. The simulated surface topography is used to predict surface roughness, whose value is acquired by the average line roughness of ten sections. The roughness of simulation and experiment is listed in Table 4.

As shown in Table 4, when feed per tooth is higher than 0.2 mm/z, the surface roughness is close to the value of experiment, and the maximum relative error is smaller than 20%. When feed per tooth is lower than 0.2 mm/z, the difference between simulation and experiment is relatively large. This may be because of the lack of accuracy of the machine tool or other unknown reasons.

Above all, the presented surface model can be used to predict the peripheral milling surface geometry as well as surface roughness.

4.3 Simulation parametric analysis and formula of surface roughness

Parametric analysis according to surface generation model is conducted to explore the influence of process parameters on

Table 3 Range of cutting parameters

Process parameters	Range	Increment
Spindle speed Ω	1000 rpm	0
Axial depth of cut a_p	1–4 mm	1 mm
Radial depth of cut a_e	0.5–2.0 mm	0.5 mm
Feed rate f	200–800 mm/min	200 mm/min

roughness. Since the simulated surface roughness has been proved to be accurate enough, the simulation surface roughness data is chosen. The growth tendency of surface roughness to different process parameters is depicted in Fig. 14.

Note that when the effect of a_p is discussed, the other parameters are fixed as follows: $a_e = 0.5$ mm, $f_t = 0.3$ mm/z. On the other side, when a_e is discussed, the other parameters are as follows: $a_p = 1$ mm, $f_t = 0.3$ mm/z. As demonstrated in Fig. 14, depth of cut a_p has little impact on the surface roughness comparing with cutting thickness a_e within the chosen range.

A more detailed parametric analysis is shown in Fig. 15 to analyze the difference in the growth trend of various parameters.

Combing the result in Fig. 14 and Fig. 15(a), the depth of cut a_p has little impact on surface roughness when a single factor is taken into account. In Fig. 15(a), (b), and (d), little interaction can be seen. In Fig. 15(c), however, axial depth of cut affects the slope of curve in a small scale, which can be inferred that a_p and a_e are not independent variables. Moreover, it can be found that the effect of these factors on surface roughness is nonlinear.

The degree of influence of each parameter on surface roughness can be observed through Fig. 15 within the specific range. Among all three parameters considered, axial depth of cut a_p has the least impact on surface roughness followed by the radial cutting depth a_e , and the feed per tooth f_t affects most on the surface roughness.

Since the value of surface roughness had already been verified in Section 4.2, the empirical equation can be deduced if interaction of a_p and a_e is ignored, as in Eq. (6).

$$S_a = 6.1505 \times a_p^{0.004} \times a_e^{0.069} \times f_t^{2.084} \tag{6}$$

where the unit of S_a is μm , a_p , a_e are mm, and f_t is mm/z. The index in the empirical formula confirms the conclusion

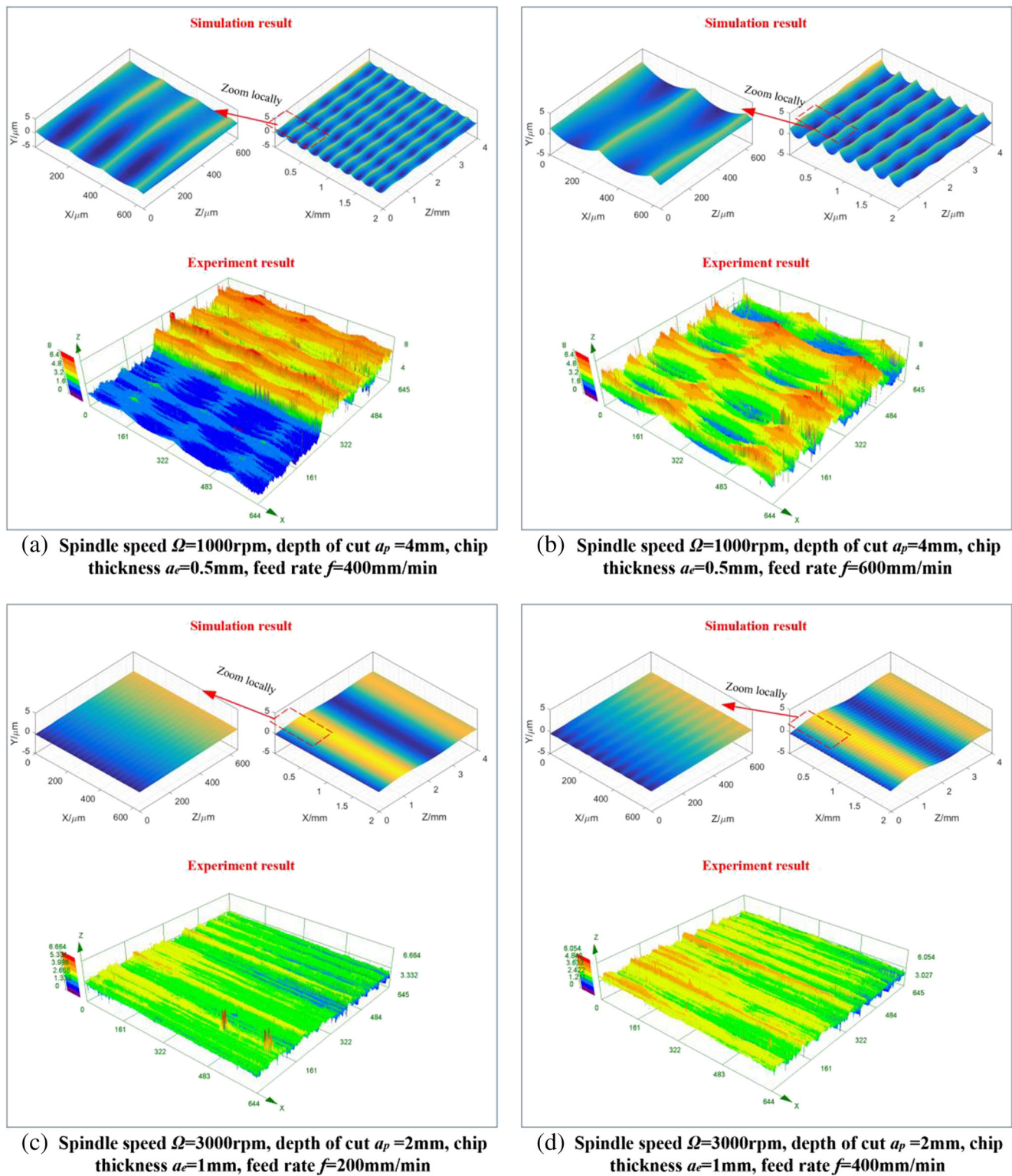


Fig. 13 Comparison of simulation and experiment results under different feed per tooth

raised above. Equation (6) can be used in machining parameter optimization when feed per tooth is larger than 0.1 mm/z and the effects of different cutting process on surface roughness are independent.

5 Conclusion

In this paper, a novel model of surface generation considering cutting force and vibration is established. The

Table 4 Surface roughness of simulation and experiments

Cutting parameters	Simulated roughness	Experimental roughness	Relative error
$a_p = 4 \text{ mm}, a_e = 0.5 \text{ mm}, f_i = 0.1 \text{ mm/z}$	0.049 μm	0.211 μm	76.78%
$a_p = 4 \text{ mm}, a_e = 0.5 \text{ mm}, f_i = 0.2 \text{ mm/z}$	0.207 μm	0.248 μm	16.53%
$a_p = 4 \text{ mm}, a_e = 0.5 \text{ mm}, f_i = 0.3 \text{ mm/z}$	0.486 μm	0.493 μm	1.42%
$a_p = 4 \text{ mm}, a_e = 0.5 \text{ mm}, f_i = 0.4 \text{ mm/z}$	0.873 μm	0.838 μm	4.18%
$a_p = 2 \text{ mm}, a_e = 1 \text{ mm}, f_i = 0.1 \text{ mm/z}$	0.050 μm	0.235 μm	78.72%
$a_p = 2 \text{ mm}, a_e = 1 \text{ mm}, f_i = 0.2 \text{ mm/z}$	0.216 μm	0.263 μm	17.87%
$a_p = 2 \text{ mm}, a_e = 1 \text{ mm}, f_i = 0.3 \text{ mm/z}$	0.513 μm	0.641 μm	19.97%
$a_p = 2 \text{ mm}, a_e = 1 \text{ mm}, f_i = 0.4 \text{ mm/z}$	0.927 μm	0.834 μm	11.15%
$a_p = 1 \text{ mm}, a_e = 2 \text{ mm}, f_i = 0.1 \text{ mm/z}$	0.051 μm	0.314 μm	83.76%
$a_p = 1 \text{ mm}, a_e = 2 \text{ mm}, f_i = 0.2 \text{ mm/z}$	0.224 μm	0.266 μm	15.79%
$a_p = 1 \text{ mm}, a_e = 2 \text{ mm}, f_i = 0.3 \text{ mm/z}$	0.535 μm	0.551 μm	2.90%
$a_p = 1 \text{ mm}, a_e = 2 \text{ mm}, f_i = 0.4 \text{ mm/z}$	0.982 μm	0.880 μm	11.59%

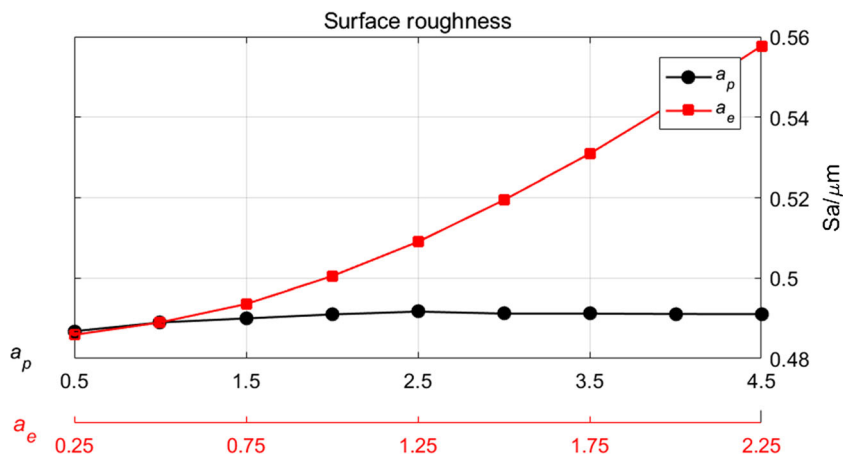
simulated surface geometry shows good consistence with that of the experiment, and the results of surface roughness in simulation are close to the experiment results. Afterwards, parametric analysis is introduced to study the influence of process parameters. The conclusions drawn from the present work are as follows.

- The cutting force coefficients in the model represent the relative hardness of the tool and workpiece and the modal parameters represent the dynamics of the machine tool. If the tool and workpiece are determined, the surface geometry can be predicted under certain cutting condition.
- The presented model can be used to predict the peripheral milling surface according to theoretical research and experiments, which can save both time and material. Furthermore, the surface roughness can be acquired under

current experimental conditions when feed per tooth f_i is over 0.2 mm/z.

- Combining the analysis of geometry and roughness, the order of impact on the surface generation is $f_i > a_e > a_p$, where feed per tooth f_i affects both feed marks and vibration amplitude, and the radial depth of cut a_e has larger impact on vibration than axial depth of cut a_p . Although the axial depth of cut has the least effect on the machined surface compared with other parameters, the effect should not be ignored when cutting thickness is relatively large.
- To acquire an ideal machined surface as well as processing efficiency, the axial depth of cut a_p may be chosen to a relatively large value. However, when the cutting stability is considered, the value of a_p should be lower than the stable limit to avoid chatter and critical condition.

Fig. 14 Growth tendency of surface roughness to different process parameters



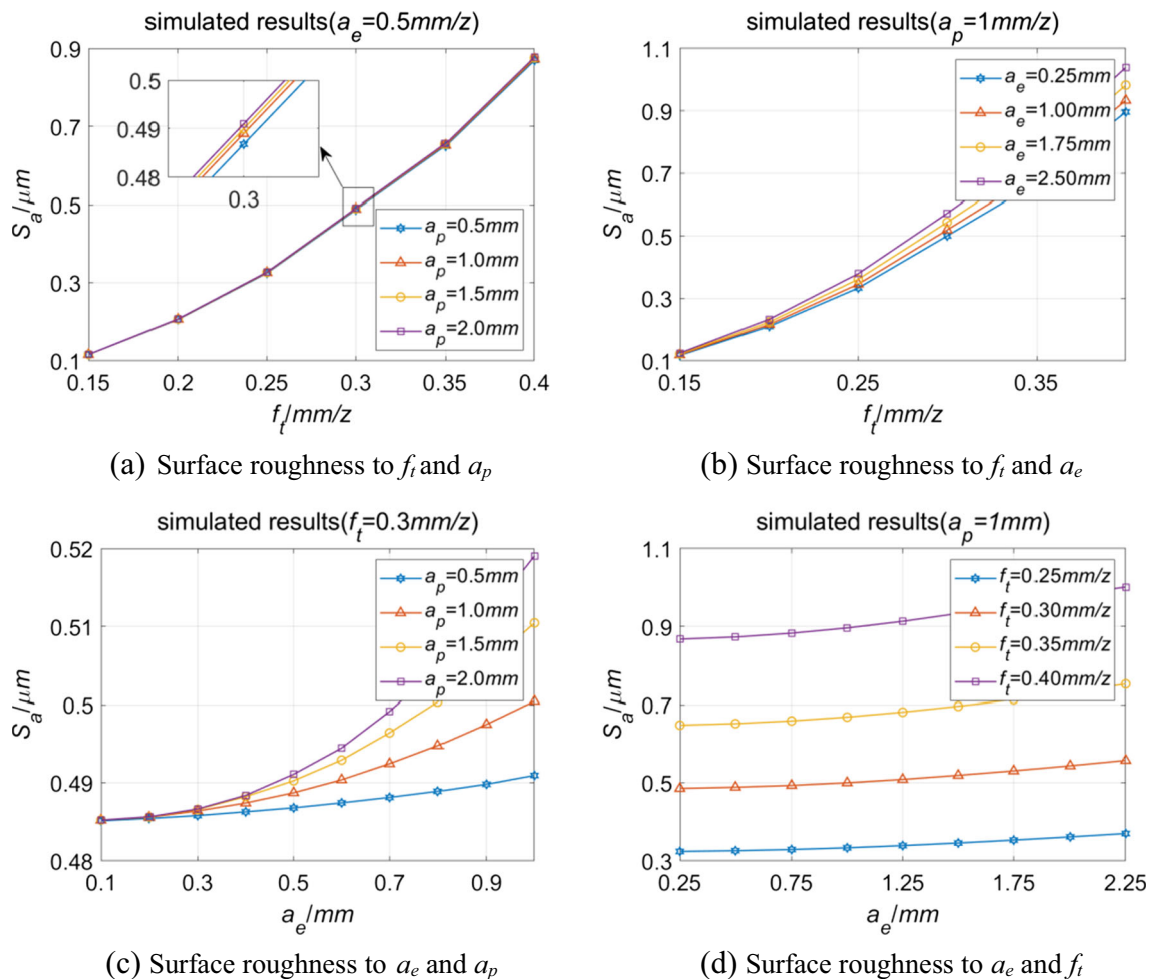


Fig. 15 Trend of surface roughness

References

- Wojciechowski S, Twardowski P, Pelic M, Maruda RW, Barrans S (2016) Precision surface characterization for finish cylindrical milling with dynamic tool displacements model. *Precis Eng* 46:158–165
- Grossi N, Scippa A, Sallase L, Montevecchi F, Campatelli G (2018) International Journal of Machine Tools and Manufacture On the generation of chatter marks in peripheral milling: a spectral interpretation. *Int J Mach Tools Manuf* 133:31–46
- Denkena B, Krüger M, Bachrathy D, Stepan G (2012) Model based reconstruction of milled surface topography from measured cutting forces. *Int J Mach Tools Manuf* 54–55:25–33. <https://doi.org/10.1016/j.ijmachtools.2011.12.007>
- Omar OEEK, El-Wardany T, Ng E, Elbestawi MA (2007) An improved cutting force and surface topography prediction model in end milling. *Int J Mach Tools Manuf* 47:1263–1275
- Yang D, Liu Z (2015) International Journal of Machine Tools & Manufacture Surface plastic deformation and surface topography prediction in peripheral milling with variable pitch end mill. *Int J Mach Tools Manuf* 91:43–53
- Cheng HD, Chen S-J, Cheng K (2011) Dynamic surface generation modeling of two-dimensional vibration-assisted micro-end-milling. *Int J Adv Manuf Technol* 53:1075–1079
- Arizmendi M, Campa FJ, Fernández J, López de Lacalle LN, Gil A, Bilbao E, Veiga F, Lamikiz A (2009) Model for surface topography prediction in peripheral milling considering tool vibration. *CIRP Ann* 58:93–96
- Arizmendi M, Jiménez A (2019) Modelling and analysis of surface topography generated in face milling operations. *Int J Mech Sci* 163:105061
- Liu C, He Y, Wang Y, Li Y, Wang S, Wang L, Wang Y (2019) An investigation of surface topography and workpiece temperature in whirling milling machining. *Int J Mech Sci* 164:105182
- Zhang G, Li J, Chen Y, Huang Y, Shao X, Li M (2014) Prediction of surface roughness in end face milling based on Gaussian process regression and cause analysis considering tool vibration. *Int J Adv Manuf Technol* 75:1357–1370
- Bolar G, Das A, Joshi SN (2018) Measurement and analysis of cutting force and product surface quality during end-milling of thin-wall components. *Measurement* 121:190–204
- Lu X, Hu X, Jia Z, Liu M, Gao S, Qu C et al Model for the prediction of 3D surface topography and surface roughness in micro-milling Inconel 718. *Int J Adv Manuf Technol* 94:2043–2056
- Karabulut Ş (2015) Optimization of surface roughness and cutting force during AA7039/Al2O3 metal matrix composites milling using neural networks and Taguchi method. *Meas J Int Meas Confed* 66:139–149. <https://doi.org/10.1016/j.measurement.2015.01.027>

14. Karkalos NE, Galanis NI, Markopoulos AP (2016) Surface roughness prediction for the milling of Ti – 6Al – 4V ELI alloy with the use of statistical and soft computing techniques. *Measurement* 90: 25–35
15. Liu N, Wang SB, Zhang YF, Lu WF (2016) A novel approach to predicting surface roughness based on specific cutting energy consumption when slot milling Al-7075. *Int J Mech Sci* 118:13–20
16. Wan M, Liang XY, Yang Y, Zhang WH (2020) Suppressing vibrations in milling-trimming process of the plate-like workpiece by optimizing the location of vibration absorber. *J Mater Process Technol* 278:116499
17. Yuan H, Wan M, Yang Y (2019) Design of a tunable mass damper for mitigating vibrations in milling of cylindrical parts. *Chinese J Aeronaut* 32:748–758
18. Ding Y, Zhu L, Zhang X, Ding H (2010) *International Journal of Machine Tools & Manufacture Short Communication* A full-discretization method for prediction of milling stability. *Int J Mach Tools Manuf* 50:502–509
19. Zhang Q, Li XGH (2017) Minimum time corner transition algorithm with confined feedrate and axial acceleration for nc machining along linear tool path. *Int J Adv Manuf Technol*:941–956
20. Eynian M (2015) Frequencies in stable and unstable milling. *Int J Mach Tools Manuf* 90:44–49
21. Caliskan H, Kilic ZM, Altintas Y. (2018) On-line energy-based milling chatter detection;140:1–12.
22. Liu C, Zhu L, Ni C (2018) Chatter detection in milling process based on VMD and energy entropy. *Mech Syst Signal Process* 105:169–182

Publisher's note Springer Nature remains neutral with regard to jurisdictional claims in published maps and institutional affiliations.